

PROGRESS IN ION BEAM ANALYSIS AT FUDAN UNIVERSITY

Yang Fujia(杨福家) and Tang Jiayong(汤家镛)

(Fudan University, Shanghai 200433, China)

(Received November 1989)

ABSTRACT

Progress in ion beam analysis at Fudan University in the recent years is briefly reviewed. Presented as examples of the research activities performed in this field are the following projects: (1) Nuclear potential resonance scattering of 6.25 MeV and 4.25 MeV helium ions for simultaneous compositional analysis of carbon and oxygen in a Mylar, a SnInO₃ and some other film samples; (2) Determination of stoichiometry of a high-temperature superconducting Y-Ba-Cu-O sample by backscattering of 8.8 MeV helium ions; (3) Backscattering and channeling analysis of multilayered structures periodically consisting of layers of pure Si and alternate layers of Ge and Si, grown on (100) Si substrates by molecular beam epitaxy; (4) Studies of surface structure of Al(100) by the use of MeV ions backscattering and channeling surface peak; and (5) MeV ion microbeam analysis and the use of PIXE method in DNA study, etc.

Keywords: Ion beam analysis Non-Rutherford backscattering Channeling analysis of superlattice Surface structure study MeV ion microbeam system

1. Introduction

A 3MV NEC 9SDH-2 tandem pelletron has been installed at Fudan^[1] since September 1987. Among the six beam stations available, three beam lines that have been established are all IBA-oriented, including an ultra-high-vacuum chamber (933.21×10^{11} Pa) used for surface and interface structure study by high energy ion scattering; an experimental apparatus for X-Y electrostatic scanning implantation of high energy ions and in situ Rutherford backscattering analysis; and a microcomputer manipulated scanning microbeam system capable of measuring PIXE and RBS spectra and secondary electron images simultaneously. Reviewed here are examples of the research activities so far performed.

2. High energy elastic backscattering of helium ions for analysis of carbon and oxygen

Nuclear potential resonance scattering of 6.25 MeV helium ions was utilized for simultaneous compositional analysis of carbon and oxygen^[2]. These enhanced non-Rutherford cross sections have increased the detection sensitivity to light elements in the presence of a large amount of heavier elements, as can be seen in the scattering energy spectra of helium ions with different energies (Fig. 1 and 2). Also

shown in the figures is the carbon content at surface/interface, resulting from a sharp resonance of 4.25 MeV helium ions scattered from carbon, which manifests an even greater sensitivity to carbon than the above-mentioned non-Rutherford backscattering around 6.25 MeV. The differential cross sections of helium ions scattered by carbon in the energy ranges 4.0–4.5 MeV and 5.8–7.0 MeV and that by oxygen in the energy range 5.5–6.5 MeV were measured at a scattering angle of $\theta_{lab} = 165^\circ$ and used in calculations.

The backscattering spectra of a Mylar/Ag film are shown in Fig. 1. In account of the step heights of carbon and oxygen together with the measured scattering cross section, the stoichiometry of the surface layer was determined to be C : O = 10 : 4.1. Similarly, the depth profile can be obtained by taking into account the variations of the scattering cross section and the stopping cross section. From the signal width of carbon and oxygen the film thickness was determined to be 3.1 μm which is greater than the probing depth of 2 MeV helium ions.

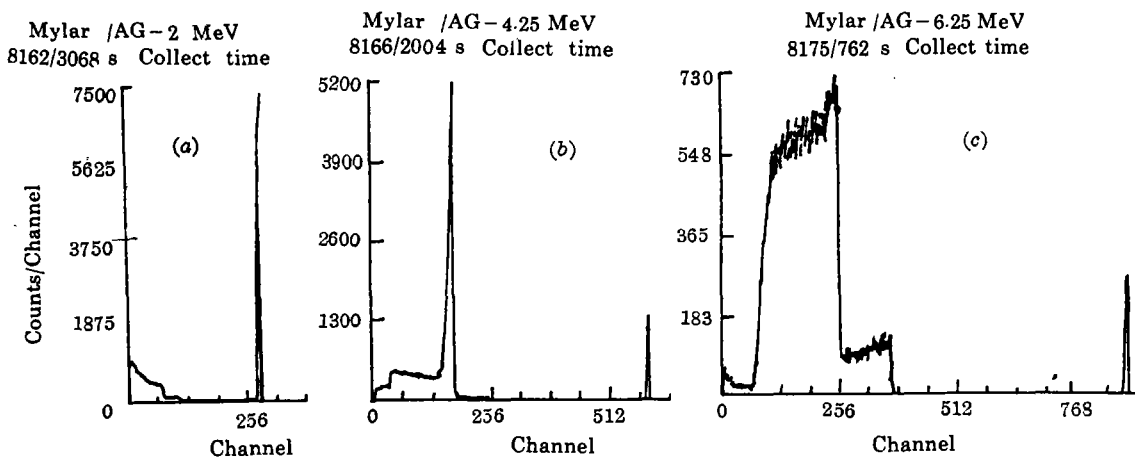


Fig.1 Backscattering spectra of 2.0 (a), 4.25 (b), and 6.25 MeV (c) helium ions from a Mylar/Ag film at an angle of $\phi_{lab} = 165^\circ$

Carbon and oxygen signals do not appear in (a), but are clearly revealed in (c)

The surface carbon peak in (b) results from the sharp resonance of 4.25 MeV ^4He ions

Fig. 2 shows the backscattering spectra from a SnInO film. Again, no carbon yet just a little oxygen appear in the spectrum measured with 2 MeV ^4He ions (Fig. 2(a)). The relative intensity of carbon and oxygen at surface in Fig. 2 (b) and Fig. 2(c) reflects the relative variation of cross sections at 4.25 and 6.25 MeV. The stoichiometry of SnIn and O was determined to be SnIn/O = 0.74, though the peaks of Sn and In could not be resolved for their small mass difference. From the peak areas of carbon in Fig. 2(b) and Fig. 2(c), the carbon contamination was determined to be 2.5×10^{16} at./cm².

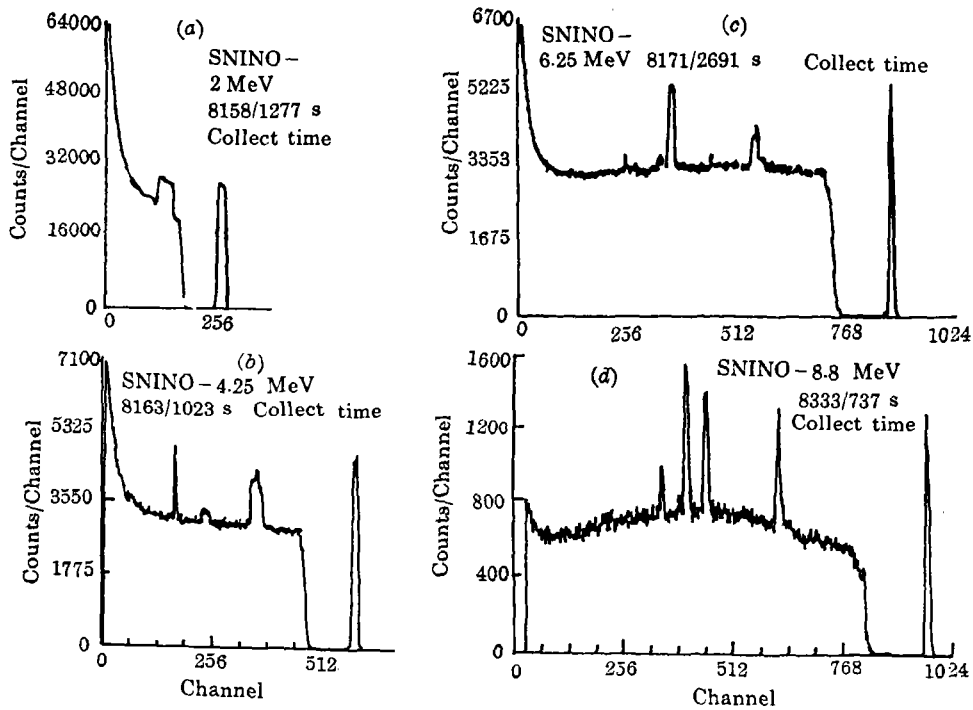


Fig.2 Backscattering spectra of ^4He ions of 2.0 (a), 4.25 (b), 6.25(c) and 8.8 MeV(d) at $\theta_{\text{lab}} = 165^\circ$ from a SnInO film on a layer of a:Si deposited on a stainless steel substrate

The oxygen peak is greatly enhanced when 6.25MeV ions were in use(c), while the carbon peak of surface contamination is still appreciable. The nitrogen peak in(d) reveals the potential use of 8.8MeV ^4He ions for nitrogen detection

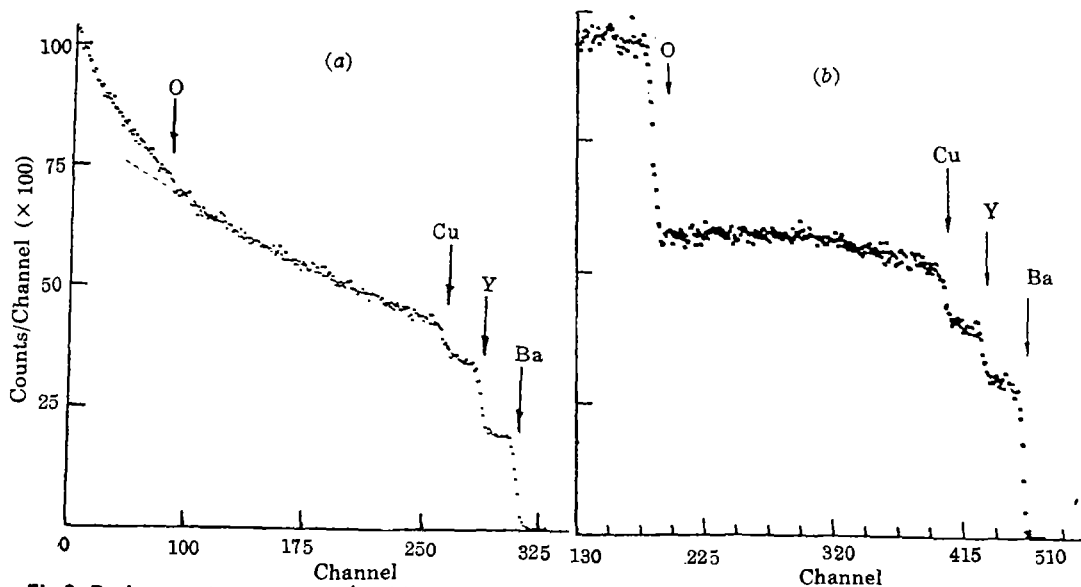


Fig.3 Backscattering spectra of $^4\text{He}^{++}$ ions of 2.0(a) and 8.8 MeV (b) from a Y- Ba- Cu- O sample

The oxygen peak is revealed by the enhanced cross section of 8.8 MeV helium ions

Also, non-Rutherford backscattering of 8.8 MeV helium ions, which has an increased sensitivity to ^{16}O by a factor of 25 over RBS^[3], was utilized to measure quantitative metal and oxygen stoichiometries in high-temperature superconducting (HTS) materials. The superiority of 8.8 MeV helium ion scattering to low energy analysis of HTS materials is clearly demonstrated in Fig.3. Direct oxygen determination using 2 MeV ^4He ions is unpractical because the oxygen cross section is low relative to the metals and the oxygen peak rests on a high background (Fig. 3(a)). The enhanced cross sections of 8.8 MeV helium ions reveals the oxygen peak drastically (Fig. 3(b)), and the stoichiometry of oxygen and metals in a Y-Ba-Cu-O sample was determined to be $\text{Y}_{1.2}\text{Ba}_2\text{Cu}_3\text{O}_{6.7}$ ^[4].

3. Ion channeling analysis of Ge-Si superlattices

Multilayered structures periodically consisting of pure Si layers and Ge/Si alternate layers, grown on (100) Si substrates by molecular beam epitaxy, were analyzed using 2 MeV ^4He ion axial channeling technique combined with RBS^[5]. In order to enhance the depth resolution of backscattering measurements, samples were tilted to 55° , and the random backscattering spectrum measured is shown in Fig. 4

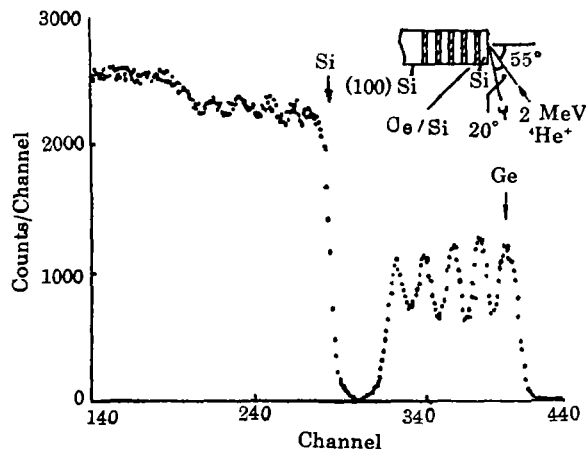


Fig.4 Glancing angle backscattering spectrum of 2 MeV helium ions for a **5[25 nm Si/10(0.4 nm Ge/0.6 nm Si)]/(100) Si superlattice sample**

for a 5[25nm Si/10(0.4nm Ge/0.6nm Si)]/(100)Si superlattice sample (Sample description: one pure Si layer of 25 nm in thickness was deposited by following an alternate Ge/Si deposition layer of 10 nm, and each Ge/Si alternate layer consisted of 10 layers (10 "small period") of 0.4 nm Ge and 0.6 nm Si. This sequence was repeated five times (5 "large period"), resulting in a total film thickness of 175 nm). Since the Ge peaks are well resolved, the thickness per pair of pure Si and Ge/Si alternate layer can be determined by the position of the maxima of these oscillating Ge peaks and the thickness of Ge/Si alternate layers can be extracted from the peak width.

Fig. 5 shows channeled spectra for the $\langle 100 \rangle$ and $\langle 110 \rangle$ axes of the same sample. Along the $\langle 100 \rangle$ growth direction the aligned spectrum is nearly identical to that for a virgin Si substrate. The $\langle 100 \rangle$ channeling result indicates a good crystalline quality of the Ge-Si superlattice studied. However, along the $\langle 110 \rangle$

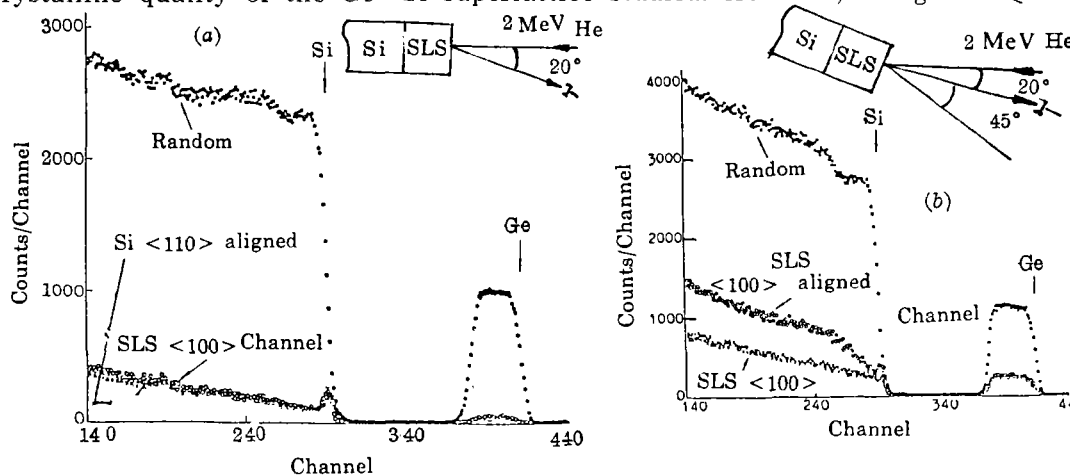


Fig.5 Random and channeling ion backscattering spectra for the sample as in Fig.4

Channeled spectra are shown for normal $\langle 100 \rangle$ axis (a), and for inclined $\langle 110 \rangle$ axis (b)

inclined direction relative to the growth direction an increase of dechanneling for the superlattice sample over that for the Si substrate is observed. It is due to the presence of the strain which results in a tilt angle relative to the inclined crystal axis at the interface between layers in strained-layer superlattices (SLS).

4. Studies of surface structure by MeV ions scattering and channeling

The use of the backscattering/channeling surface peak in surface structure analysis was introduced about a decade ago^[6]. Taking the advantage of an UHV chamber with a variety of surface characterization tools, which was designed and assembled at

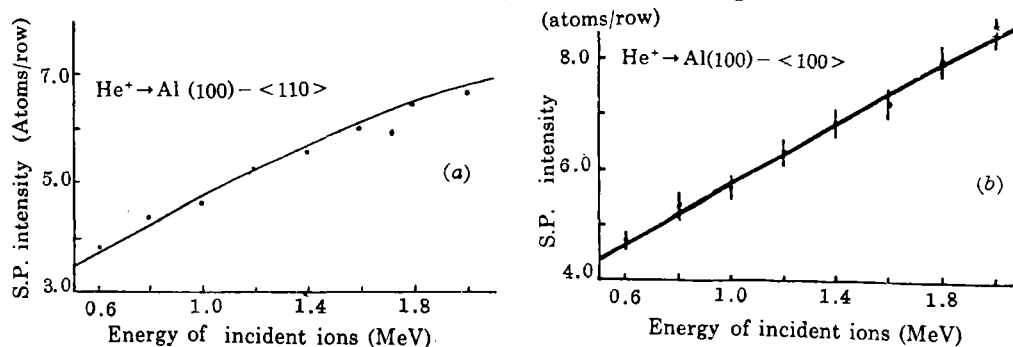


Fig.6 Energy dependence of surface peak intensity for clean Al(100) surface

(a) in $\langle 100 \rangle$ incidence. Solid curve is the computer simulation assuming a bulk-like structure with $u = 0.0096$ nm, $\sigma = 0.2$, and $c = 1.2$ (first layer) and 1.1 (second layer)

(b) in $\langle 110 \rangle$ incidence; assuming a bulk-like structure with $u = 0.0096$ nm, $\sigma = 0.3$, and $c = 1.3$ (first layer) and 1.15 (second layer)

SUNY/Albany and later found its new home at Fudan, we started surface structure study right after the pelletron was installed. Used in the first experiment^[7] was a high-purity Al(100) sample. Alternate treatment of argon ion sputtering and annealing for more than 10 hours was needed to reach a clean Al(100)-(1×1) structure.

Energy dependence of surface peak intensity was measured on a clean Al(100) surface, either in $\langle 100 \rangle$ incidence or in $\langle 110 \rangle$ incidence. The experimental results were then compared with the calculations of computer simulation, taking the one-dimensional rms amplitude of thermal vibration u , the correlation coefficient of neighbouring atoms α , and the enhanced factor of thermal vibration of surface atoms ϵ as fitting parameters (Fig. 6 a,b).

Fig. 7 is the angular dependence of $\langle 110 \rangle$ surface peak intensity at $E_n = 1.0$ MeV for a clean Al(100)-(1×1) structure. The uncertainty of measurements, shown by the error bars, was estimated to be $\pm 4\%$. Solid and dashed curves show the results of computer simulations in which a bulk-like structure and a uniform expansion of the first layer by -0.005 nm (inward) are assumed, respectively. It was the first time that the surface relaxation of Al(100) was experimentally identified.

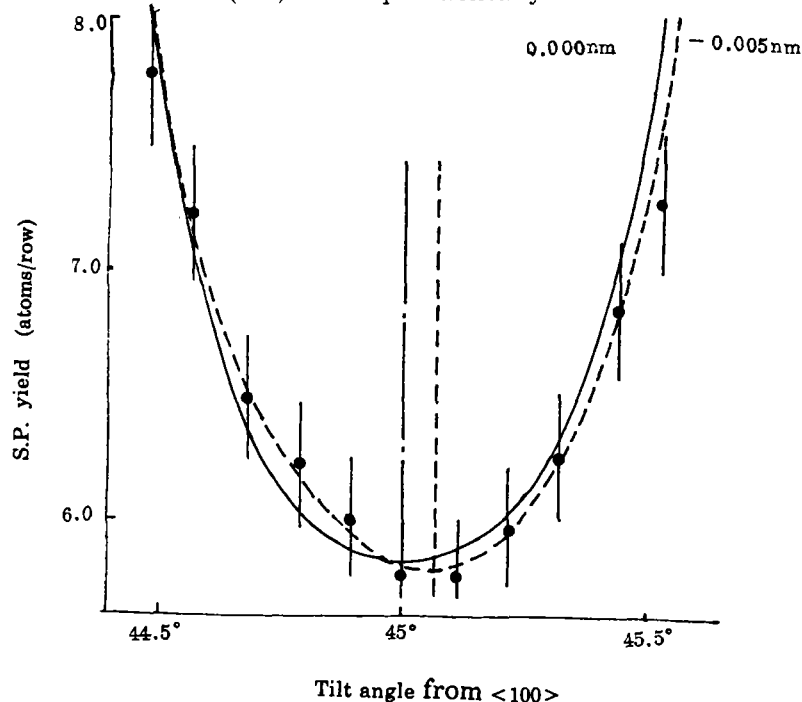


Fig.7 Angular dependence of $\langle 110 \rangle$ surface peak intensity at $E_n = 1.0$ MeV for a clean Al(100) surface

Solid and dashed curves correspond to the computer simulations of a bulk-like structure and a relaxation surface, respectively

5. MeV ion microbeam analysis and other PIXE-associated topics

Another close collaboration with SUNY/Albany is a nuclear microprobe. It started running in May 1988, the first microbeam facility operating in China. With a microcomputer manipulated scanning system and a data acquisition system, PIXE and RBS spectra, and secondary electron images can be measured, and three-dimensional distributions of elemental composition can be displayed. Part of the first experimental results^[4] is given in Fig.8. Since then, this beam line has been shortened and rearranged for better optics. Recent measurements were made with a beam size of $\sim 3 \mu\text{m}$ and a beam current of 100–300 pA. Shown in Fig. 9 are 3-dimensional maps of elemental composition for a creep crack in steel.

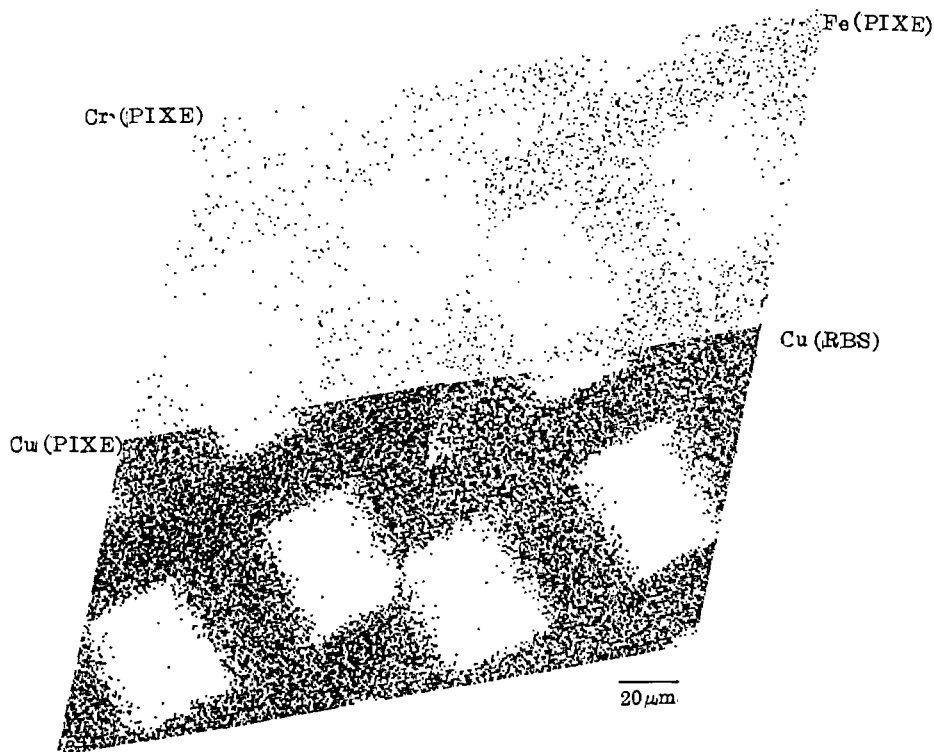


Fig.8 2-dimensional maps of Cr, Fe, and Cu for a 400 mesh copper grid

Size: $100 \times 100 \mu\text{m}$ Measuring time: about 1 h Date: 1988.4.28

PIXE analytical technique has been widely used in Fudan and applied to a variety of research fields, such as archaeology and biology (pathology) studies, environment

monitoring, etc. Other PIXE-associated topics include PIXE induced XRF technique and its application, paper deterioration caused by proton bombardment, and the use of PIXE method in DNA study. Only the DNA study will be quoted as an example, in which an external beam proton system, improved in its detection sensitivity, was used. In the study⁽⁹⁾, a metal-organic compound $\text{Ru}(\text{DiP})_3^{2+}$ was used to distinguish the different conformations of DNA and locate the regulatory regions of a gene, and hence acted as a metal marker of DNA. The labeled DNA was then electrophoresed in an agarose gel. The interesting DNA samples with intercalated $\text{Ru}(\text{DiP})_3^{2+}$ showed clearly Ru peaks in the PIXE spectra, while the control showed no Ru peaks at all. The interesting conformations of DNA or the regulatory regions of a gene can thus be identified.

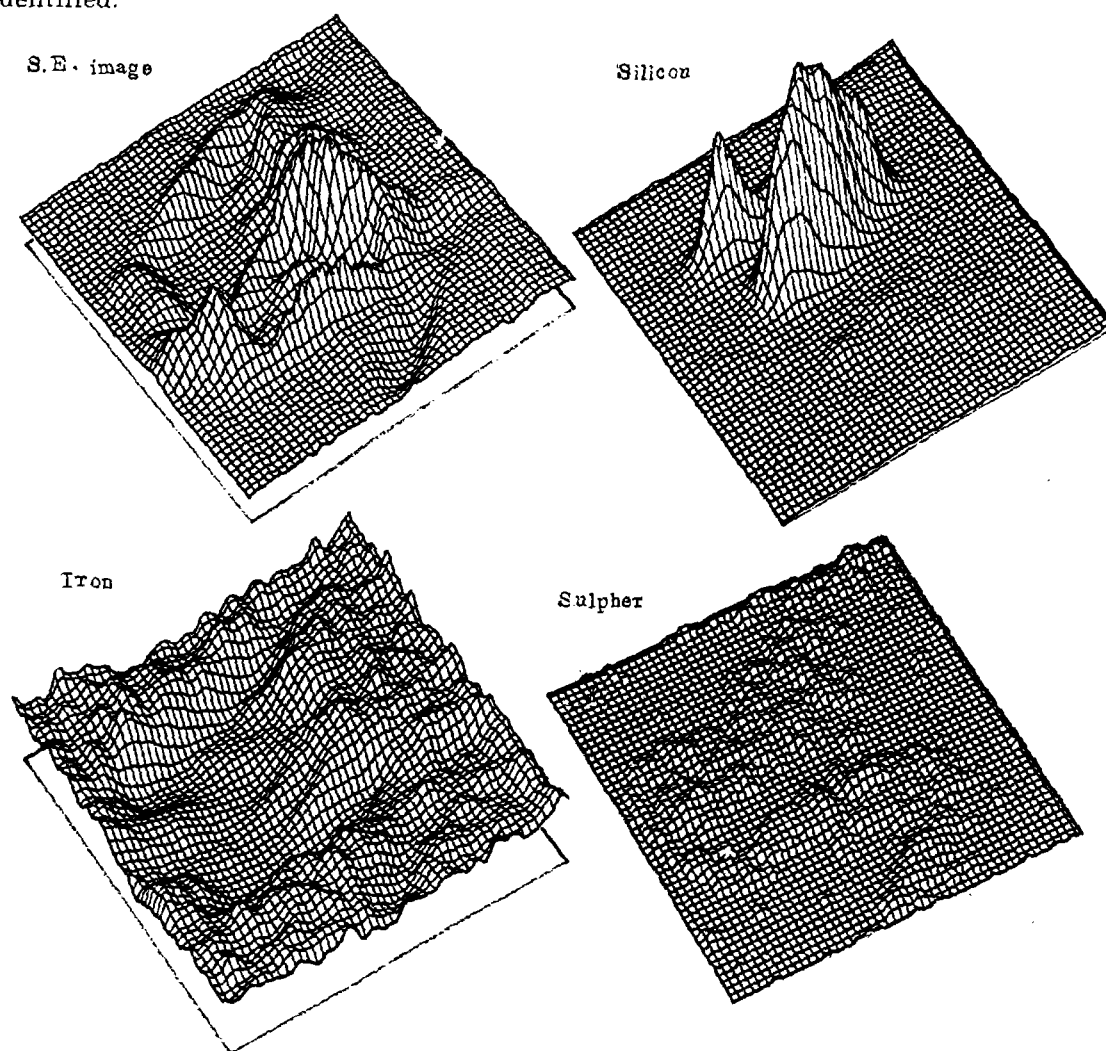


Fig.9 3- dimensional maps

REFERENCES

- [1] Sun C.C. et al., *Nucl. Instr. Meth.*, **B40/41** (1989), 714.
- [2] Zhou Z.Y. et al., to be presented at the 9th intl. conf. on ion beam analysis, Kingston, Canada, June 1989.
- [3] J.A. Martin et al., *Appl. Phys. Lett.*, **52** (1988), 25 : 2177.
- [4] Cheng H.S. et al., *Nucl. Tech.*, (Shanghai) to be published, 1989.
- [5] Zhao G.Q. et al., *Solid Communications*, **67** (1988), 6 : 661.
- [6] See, for instance, L.C. Feldman, *Nucl. Instr. Meth.*, **191** (1981), 211.
- [7] Cheng H.S. et al., *Acta Phys. Sin.*, **38** (1989), 12 : 1981.
- [8] Ren C.C. et al., Proc. of the 2nd national conf. on microbeam analysis, F-17 & F-21, Wuhan, China, 1988.
- [9] Sun Y.N. et al., Presentation at the int. symposium on appl. of nucl. tech., Shanghai, China, May 1989.